Tip geometry effects in scanning capacitance microscopy on GaAs Schottky and metal-oxide-semiconductor-type junctions

C. Eckhardt,[a] W. Brezna, O. Bethge, E. Bertagnolli, and J. Smoliner[b]
Institut für Festkörperelektronik, TU-Wien, Floragasse 7, A-1040 Wien, Austria

(Received 10 February 2009; accepted 1 May 2009; published online 8 June 2009)

In this work, the influence of the tip geometry in scanning capacitance microscopy is investigated experimentally and theoretically on metal-oxide-semiconductor- (MOS) and Schottky-type junctions on gallium-arsenide (GaAs). Using a two-dimensional model we find that on Schottky-type junctions the electric field around the tip is screened by the surface states and that the essential parameters entering the capacitance versus voltage $C(V)$ characteristics are the doping level and the contact area only. In contrast to that, the electric field from the tip penetrates into the semiconductor on a MOS-type junction, and the tip geometry effects are much larger. $C(V)$ spectra are fitted to the experimental data and allowed a quantitative determination of doping levels, oxide thickness, and contact area without further calibration measurements. © *2009 American Institute of Physics*. [DOI: 10.1063/1.3140613]

I. INTRODUCTION

Nowadays, scanning probe microscopy is routinely used in a wide area of applications ranging from basic research to industrial quality control. Among the vast number of different scanning probe methods, atomic force microscopy with conducting tips (cAFM) is especially helpful to investigate nanostructures,[1,2] local properties of dielectric films,[3–6] and recently also organic films.[7] The cAFM technique we want to discuss in this paper is scanning capacitance microscopy (SCM). In SCM, a conductive AFM tip is used to measure the local capacitance between the tip and the sample. In scanning capacitance spectroscopy (SCS), the capacitance is recorded during a dc voltage sweep to obtain a capacitance versus voltage $C(V)$ curve for further analysis. The main application of this method is two-dimensional carrier profiling for failure analysis or process control especially on cross sectional samples.

Although SCM and SCS already had been used for many years, quantitative SCM/SCS measurements are still a major challenge for technical and physical reasons. First, the measured capacitance values are in the sub-fF regime only, and to obtain a reasonable signal size at reasonable data collection speed for imaging, lock-in techniques are normally used. Thus, commercial SCM systems usually yield qualitative dC/dV data only. A survey about this technique can be found in the review articles,[8,9] for example.

To obtain quantitative results using commercial SCM systems, the qualitative dC/dV data have to be calibrated. This, however, is technically complicated due to large difficulties with the reproducibility of the reference sample preparation process.[10–12] In addition, the properties of the SCM tip–sample contact (e.g., the tip diameter) has a large impact on the experimental $C(V)$ or dC/dV data. Therefore, the results strongly vary between experiments with different SCM tips.

In this paper, we want to show the influence of the AFM tip geometry both for Schottky-type and metal-oxide-semiconductor (MOS)-type junctions on gallium-arsenide (GaAs) using a two-dimensional self-consistent Poisson solver. The results are compared with experimental data and allow a quantitative extraction of various physical parameters without using calibration samples.

II. EXPERIMENTAL

The samples we use for our studies were Schottky-type and MOS-type junctions on *n*-doped GaAs ($N_D = 1 \times 10^{16}$ cm^{-3} confirmed by Hall measurements). The Schottky contacts are established between the conducting tip of the AFM and the bare GaAs surface; for the MOS junctions, a high-*k* dielectric layer of Al_2O_3 was used as insulator. To obtain a good oxide quality, the Al_2O_3 has been grown by atomic layer deposition (ALD) at temperatures of 200 °C from trimethylaluminum and water precursors. On our samples, the oxide thickness was 1 nm (determined by ellipsometry). Prior to the deposition, all substrates have been exposed to ammonium hydroxide (NH_4OH) for 3 min to remove the native oxide and leave a hydroxylated GaAs surface.[13] After oxide deposition, rapid thermal annealing in inert N_2 atmosphere has been applied for a duration of 30 s at 600 °C. Typically, these films have a dielectric constant[14] of $k=9$ and a bandgap of 8.7 eV and are amorphous[15] up to processing temperatures of 850 °C.

All SCM measurements where carried out using a Digital Instruments DI3100 atomic force microscope. For quantitative SCS an ultrahigh precision, low frequency (1 kHz) capacitance bridge (AH 2550 by Andeen Hagerling) was attached to the AFM. For all measurements, a modulation voltage of 125 mV was used. More details about the setup used for quantitative SCS can be found in our previous publications.[16,17]

As AFM cantilevers we used AFM tips from NanoWorld, which were coated with highly doped (*p*-type, $N_A = 1 \times 10^{20}$ cm^{-3}) conductive diamond. Typically, the tips

[a]Electronic mail: christian.eckhardt@tuwien.ac.at.
[b]Electronic mail: juergen.smoliner@tuwien.ac.at.

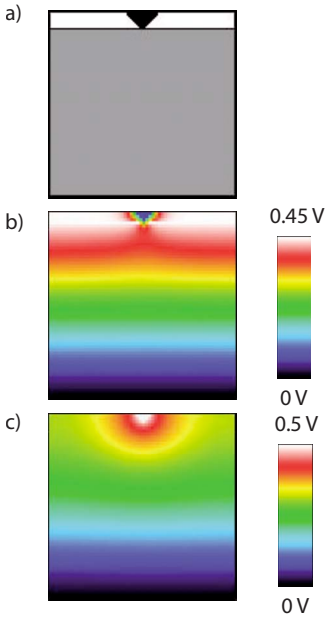

FIG. 1. (Color online) (a): Sample geometry as used for our simulation. The lower (gray) area represents the GaAs substrate; on top we have a layer of aluminum oxide (MOS-type contact) or the bare GaAs surface in case of a Schottky contact. The white area indicates air ($\varepsilon=1$) and the tip-apex is represented by the black triangle. (b) Typical potential distribution of a Schottky-type contact and (c) a MOS-type contact. The area of this plot is $1\times1\ \mu m^2$.

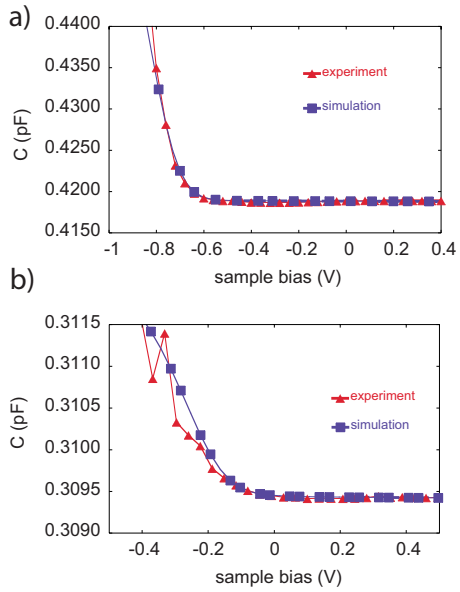

FIG. 2. (Color online) Measured and calculated $C(V)$ curves of Schottky-type tip-sample contacts on GaAs substrates with doping concentrations of (a) $N_D=1\times10^{16}$ cm^{-3} and (b) $N_D=1\times10^{17}$ cm^{-3}, respectively. The parasitic background capacitance, which always exists between the large tip-holder and the sample, was added as a fitting parameter.

have a pyramidal shape with side angle of approximately 45° according to the datasheet. The "tip radius" is specified to be below 100 nm. As we will show later, however, we find a typical contact area of 30×30 nm^2.

III. RESULTS AND DISCUSSION

In Fig. 1(a) we show the two-dimensional sample geometry, which was used for our simulations. The lower (gray) area represents the GaAs substrate. On top we have a layer of Al_2O_3 grown by ALD (MOS-type contact) or the bare surface (Schottky contact). The white area indicates air and the tip-apex is represented by the black triangle. To determine the potential distribution, a self-consistent Poisson solver employing a finite element method[18] (FEM) was used. The size of the simulation area is $1\times1\ \mu m^2$ and the size of the discretization mesh was 400×400 points. In Fig. 1(b) the potential distribution is illustrated for a Schottky-type contact and in Fig. 1(c) a MOS-type contact. In the above figures, a color scheme was used which ranges from $-U_{max}$ (black) through reverse rainbow colors to $+U_{max}$ (white).

We first discuss the results for the potential distribution for the Schottky-type contact. To model the Schottky contact, we assumed a Schottky barrier height of 0.45 V [determined by $I(V)$ measurements[19]] between the diamond tip and the GaAs. For the bare surface without tip-sample contact, a surface state induced midgap-pinning was assumed everywhere, leading to a constant value for the surface barrier height of $V_b=0.7$ V. Figure 1(b) shows the corresponding potential distribution in the n-type GaAs substrate ($N_D=1\times10^{16}$ cm^{-3}) for a tip-bias of 0.3 V and 0 V on the back contact. One can see nicely that due to the chosen boundary conditions, only the areas below the tip-apex effects the local potential distribution in the semiconductor and that the field arising from sidewalls of the tip are shielded by the surface states.

Figure 1(c) shows a MOS-type tip-sample contact with a voltage of 0.5 V applied to the tip and zero substrate bias. For the simulation of the MOS contact in Fig. 1(c), no surface states, oxide-traps, and oxide-semiconductor interface-traps were included. For the calculation of potential distribution the substrate doping was the same as in Fig. 1(b), and we further assumed a tip contact area of 50×50 nm^2, an opening angle of the apex of 45°, and an oxide layer thickness of 1 nm, identical to the measured oxide thickness on our samples. The relative dielectric constant of ALD grown Al_2O_3 films is $\varepsilon_r=9$. As one can see, the potential distribution in the substrate for the MOS system is clearly different compared to Fig. 1(b). Now, the potential distribution in the semiconductor is affected by the tip as a whole either directly in the contact area or indirectly via the $\varepsilon=1$ environment. More details on this calculation will be discussed later in this paper.

To understand the spectroscopic behavior of out capacitance data, low frequency $C(V)$ curves of Schottky-type tip-sample contacts and MOS-type tip-sample contacts were also calculated using the two-dimensional self-consistent Poisson solver using the principles outlined in Refs. 20 and 21. Any high frequency effects were ignored in our simulations. The results of the $C(V)$ calculations in the Schottky case are discussed first.

In Fig. 2 we have plotted the $C(V)$ curves of Schottky-type tip-sample contacts on GaAs substrates with doping concentrations of (a) $N_D=1\times10^{16}$ cm^{-3} and (b) $N_D=1\times10^{17}$ cm^{-3}, respectively. The triangles represent the experimental data; the rectangles represent the simulated data using a Schottky barrier height of 0.45 V (see Ref. 19). The

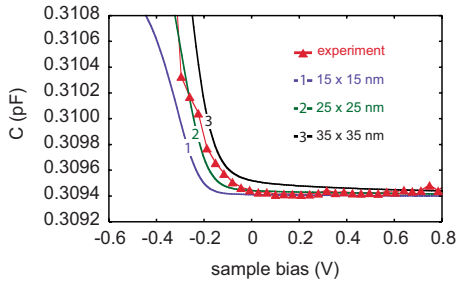

FIG. 3. (Color online) Typical $C(V)$ curve of a Schottky-type tip-sample contact on a GaAs substrate ($N_D=1\times10^{16}$ cm^{-3}). The simulated curves show the influence of the apex contact size.

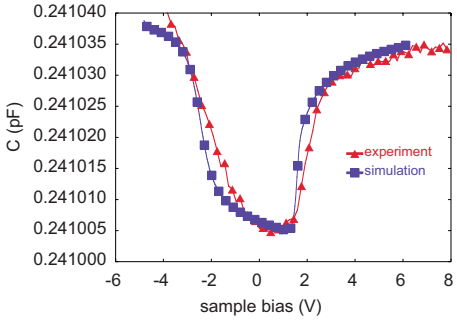

FIG. 4. (Color online) $C(V)$ curves of a MOS-type tip-sample contact with Al_2O_3 oxide layer ($d=1$ nm). Substrate doping is $N_D=1\times10^{16}$ cm^{-3}.

experimental curve is an average over 25 single curves acquired at the same position. Note that $C(V)$ curves are superimposed on a huge parasitic background capacitance, which always exists between the large tip-holder and the sample. In our simulations this huge parasitic background capacitance was added as a fitting parameter.

As one can see, the calculated and experimental curves match very well for both doping levels. It must be pointed out, however, that the good agreement in Fig. 2(b) between the experiment and the simulated $C(V)$ curves was only achieved after a very thin ($d=0.2$ nm) insulating layer of oxide between tip and sample was introduced. Without this layer, the slope of the calculated $C(V)$ curves was always much too steep for all parameters within the physically reasonable range. In our opinion, this finding is consistently explained by assuming a slightly contaminated sample. For AFM measurements in ambient atmosphere it is well known that depending on surface preparation and the age of the sample, native oxides, water films, and other contaminations are frequently present. Thus, the assumption of an insulating layer on top of the sample surface is absolutely realistic.

Figure 3 shows the results of our simulation for Schottky-type tip-sample contacts using different tip-apex contact areas as a parameter: for curve (1) a tip area of 15×15 nm^2 was used; for curve (2), 25×25 nm^2; and for curve (3), 35×35 nm^2. For the substrate doping, a value of 1×10^{16} cm^{-3} was used. As above, the parasitic background capacitance was added as a fitting parameter. The line marked with triangles represents the experimental data, and one can see that the agreement between simulation and experiment is best for a tip-apex area of approximately 30×30 nm^2. Looking at the systematic behavior of the curves as a function of contact size, mainly two things are obvious; first, the onset of the curves is shifted to the left for smaller contact area, and also the slope of the curves below the onset becomes smaller, which can be interpreted in a way that for smaller contact areas, the space charge region in the semiconductor disappears later but more abruptly.

We now discuss the results for the MOS-type tip-sample contacts. Figure 4 shows the experimentally measured $C(V)$ curve (indicated by triangles) of a MOS-type tip-sample contact with a substrate doping of 1×10^{16} cm^{-3} and a 1 nm Al_2O_3 oxide layer. The experimental curve is an average of 22 single curves. As first essential feature it has to be pointed out that in the MOS case, low frequency $C(V)$ spectra are always observed on GaAs, although the capacitance measurements are carried out at a frequency of 1 kHz. This observation is quite unusual compared to the literature results found on silicon. On macroscopic silicon MOS devices, the transition from low-frequency to high frequency behavior is already observed at low frequencies between 10 and 100 Hz, and in our previous SCS experiments on silicon samples,[22,23] we always observed the typical high frequency behavior too. For reference purposes, macroscopic $Al/Al_2O_3/n$-GaAs capacitors were therefore fabricated on the same substrates as they were used for the AFM measurements, but to our surprise, those capacitors also exhibited a clear high frequency behavior. Although we cannot offer an explanation for this discrepancy at the moment, it is no restriction for the geometry effects we want to discuss in this paper. Frequency dependent studies to clarify this behavior will be the subject of future investigations.

As one can see in Fig. 4, a quite nice agreement between the simulation and the experimental data can be achieved, provided an appropriate set of parameters is used. For a best fit between the simulated $C(V)$ curve (indicated by squares) and the experimental data, the contact area was assumed to be 50×50 nm^2. As earlier, the parasitic stray capacitance was added as a fitting parameter. Note that the position of the $C(V)$ spectrum on the voltage axis is mainly determined both by the work functions of the p-type diamond (5.8 eV) and the n-GaAs (4.53 eV at a doping level of 1×10^{16} cm^{-3}) and in addition, the number of oxide charges in the Al_2O_3. As a result of our calculation we obtain an oxide charge density of 6.3×10^{13} cm^{-2}, which is roughly a factor of ten higher compared to the ZrO_2 films in our previous publication.[17]

Figure 5(a) shows various $C(V)$ curves of a MOS-type tip-sample contact for various tip-apex-contact areas ranging from (1) 30×30 nm^2, (2) 40×40 nm^2, (3) 60×60 nm^2, to (4) 70×70 nm^2. The simulated 50×50 nm^2 curve (as shown in Fig. 3) was omitted in this plot for better clarity. As one can see in Fig. 5(a), the $C(V)$ curve saturates due to accumulation conditions at high negative sample bias; at high positive sample bias, inversion is achieved. In addition to that, the influence of contact area is quite dominant. For decreasing contact area, the minimum in the $C(V)$ curve becomes less pronounced and the corresponding region of the $C(V)$ curve becomes broader. Moreover, inversion conditions underneath the tip are moved to more positive sample bias with decreasing contact area. As seen in Fig. 4, best agree-

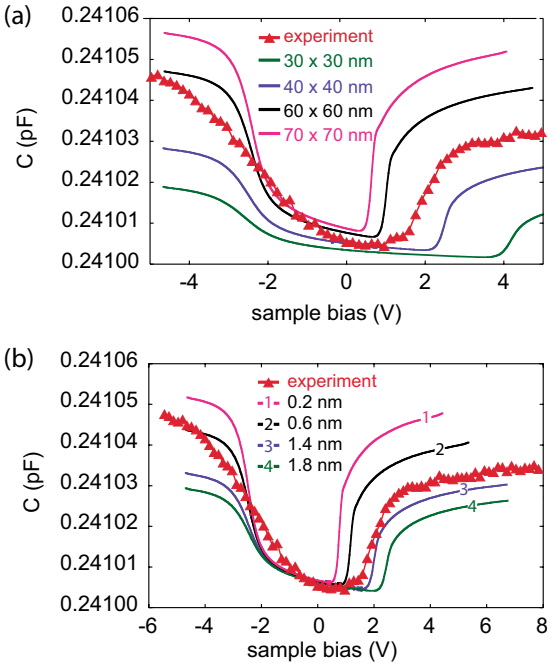

FIG. 5. (Color online) Simulated $C(V)$ curves of a MOS-type tip-sample contact for various tip-apex-contact areas: (1) 30×30, (2) 40×40, (3) 60×60, and (4) 70×70 nm^2. (b) Simulated $C(V)$ curves as a function of oxide layer thickness between 0.2 and 1.8 nm. The triangles indicate the experimental data.

ment between experiment and simulation is achieved for a tip area of 50×50 nm^2 and oxide thickness of 1 nm.

Figure 5(b) illustrates the influence of oxide thickness. For the simulated curves an oxide layer thickness of (1) 0.2, (2) 0.6, (3) 1.4, and (4) 1.8 nm and a tip contact area of 50×50 nm^2 were used. The simulated 1 nm curve (see Fig. 4) was omitted for better clarity. As one can see, the oxide thickness has a significant influence too, which is not surprising, since the oxide layer thickness is roughly in the same order of magnitude as the tip width. As expected, the depth of the minimum of the $C(V)$ curve, which is due to the influence of the space charge region underneath the tip, decreases with increasing oxide thickness. In addition, inversion conditions are shifted to higher bias values.

Figure 6 shows simulated $C(V)$ curves of a MOS-type tip-sample contact for doping concentrations between $N_D=1\times10^{17}$ and 1×10^{15} cm^{-3} together with the experimental data ($N_D=1\times10^{16}$ cm^{-3}), which are indicated by triangles. With decreasing doping concentration, the space charge region increases rapidly and leads to a more pronounced minimum in the $C(V)$ curve. In addition, accumulation appears at more negative sample bias.

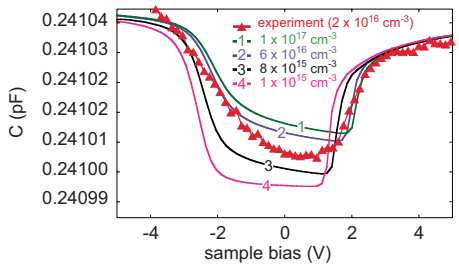

FIG. 6. (Color online) Calculated $C(V)$ curves of a MOS-type tip-sample contact for doping concentrations of (1) $N_D=1\times10^{17}$, (2) 6×10^{16}, (3) 8×10^{15}, and (4) 1×10^{15} cm^{-3}. The triangles indicate the experimental data (1×10^{16} cm^{-3}).

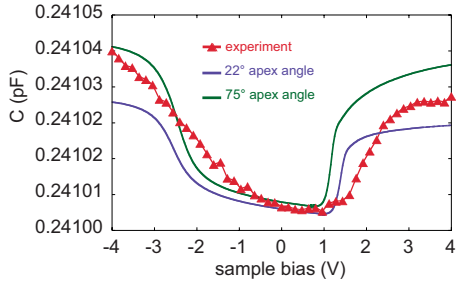

FIG. 7. (Color online) Calculated $C(V)$ curves of a MOS-type tip-sample contact for various opening angles of the tip-apex. The triangles indicate the experimental data.

Figure 7 illustrates the influence of different tip opening angles for a MOS-type tip-sample contact: (1) 22° and (2) 75°. Again the doping concentration was 1×10^{16} cm^{-3}. The triangles indicate the experimental curve with a tip-apex angle of 45°. As one can see, the capacitance under accumulation and inversion conditions decreases for smaller angles because a sharper apex tip has a smaller "effective" area. The behavior of the depth of the capacitance minimum and the broadening of the curve is obviously a combination of the effects shown in Fig. 5(a) (various tip-apex areas) and Fig. 5(b) (various oxide layer thickness).

IV. SUMMARY

In summary we have illustrated the influence of the tip geometry in SCM both for MOS-type and Schottky-type tip-sample contacts. Using a two-dimensional self-consistent Poisson solver we find that on Schottky-type junctions, the electric field around the tip is screened by the surface states and that the essential parameters entering the $C(V)$ characteristics are the doping level and the tip contact area only. In contrast to that, the electric field from tip penetrates into the semiconductor on a MOS-type junction, and the tip geometry effects are much larger. Low frequency $C(V)$ spectra that are fitted to the experimental data show an excellent agreement and allow a determination of substrate doping levels oxide thickness and oxide charge density without further calibration measurements.

ACKNOWLEDGMENTS

The authors are grateful to J. Weinbub, T. Grasser, and H. Kosina (Institut für Mikroelektronik, TU-Wien) for fruitful discussions and support. We also wish to thank S. Birner (Walter Schottky Institut, TU-München) for giving us insight into the code of the NEXTNANO3 simulation program.

This work was sponsored by "Fonds zur Förderung der wissenschaftlichen Forschung" (FWF Austria) under Project No. SFB-25-08.

[1]I. Tanaka, I. Kamiya, H. Sakaki, N. Qureshi, S. J. Allen, Jr., and P. M. Petroff, Appl. Phys. Lett. **74**, 844 (1999).
[2]I. Tanaka, E. Kawasaki, O. Ohtsuki, K. Uno, M. Hara, H. Asami, and I. Kamiya, Surf. Sci. **532–535**, 801 (2003).
[3]M. Porti, S. Meli, M. Nafría, and X. Aymerich, Microelectron. Reliab. **43**,

1203 (2003).
[4]X. Blasco, M. Nafria, X. Aymerich, and W. Vandervorst, Electron. Lett. **41**, 719 (2005).
[5]C. Sire, S. Blonkowski, M. J. Gordon, and T. Baron, Appl. Phys. Lett. **91**, 242905 (2007).
[6]S. Kremmer, C. Teichert, E. Pischler, H. Gold, K. Kuchar, and M. Schatzmayr, Surf. Interface Anal. **33**, 168 (2002).
[7]O. Douheret, A. Swinnen, M. Breselge, I. Van Severen, L. Lutsen, D. Vanderzande, and J. Manca, Microelectron. Eng. **84**, 431 (2007).
[8]V. V. Zavyalov, J. S. McMurray, and C. C. Williams, Rev. Sci. Instrum. **70**, 158 (1999).
[9]P. De Wolf, R. Stephenson, T. Trenkler, T. Clarysse, T. Hantschel, and W. Vandervorst, J. Vac. Sci. Technol. B **18**, 361 (2000).
[10]J. J. Kopanski, J. F. Marchiando, and B. G. Rennex, J. Vac. Sci. Technol. B **20**, 2101 (2002).
[11]F. Giannazzo, D. Goghero, and V. Raineri, J. Vac. Sci. Technol. B **22**, 2391 (2004).
[12]F. Giannazzo, V. Raineri, S. Mirabella, G. Impellizzeri, F. Priolo, M. Fedele, and R. Mucciato, J. Vac. Sci. Technol. B **24**, 370 (2006).
[13]Y. Xuan, H. C. Lin, and P. D. Ye, IEEE Trans. Electron Devices **54**, 1811 (2007).
[14]M. Wu, Y. I. Alivov, and H. Morkoc, J. Mater. Sci.: Mater. Electron. **19**, 915 (2008).
[15]S. Jakschik, U. Schroeder, T. Hecht, M. Gutsche, H. Seidl, and J. W. Bartha, Thin Solid Films **425**, 216 (2003).
[16]W. Brezna, M. Schramboeck, A. Lugstein, S. Harasek, H. Enichlmair, E. Bertagnolli, E. Gornik, and J. Smoliner, Appl. Phys. Lett. **83**, 4253 (2003).
[17]J. Smoliner and W. Brezna, Rev. Sci. Instrum. **78**, 106104 (2007).
[18]J. Burkardt, Finite Element Solution of the 2D Poisson Equation online book, 2007 (http://people.sc.fsu.edu/~burkardt/cpp_src/fem2d_poisson/fem2d_poisson.html).
[19]W. Brezna and J. Smoliner, J. Appl. Phys. **104**, 044309 (2008).
[20]E. H. Nicollian and J. R. Brews, *MOS (metal oxide semiconductor) Physics and Technology* (Wiley, New York, 1982).
[21]S. M. Sze, *Physics of Semiconductor Devices* (Wiley, New York, 1981).
[22]W. Brezna, S. Harasek, A. Lugstein, T. Leitner, H. Hoffmann, E. Bertagnolli, and J. Smoliner, J. Appl. Phys. **97**, 093701 (2005).
[23]S. Abermann, W. Brezna, J. Smoliner, and E. Bertagnolli, Microelectron. Eng. **83**, 1055 (2006).